Nuclear Materials and Energy 38 (2024) 101593

Contents lists available at ScienceDirect

Nuclear Materials and Energy

journal homepage: www.elsevier.com/locate/nme

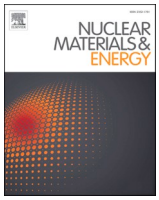

The use of time-of-flight neutron Bragg edge imaging to measure the residual strains in W/Cu dissimilar joints for fusion reactors

Omar Mohamed [a], Bin Zhu [a], Nathanael Leung [a], Winfried Kockelmann [b], Thomas R. Barrett [c], Mark J. Whiting [a], Yiqiang Wang [c], Tan Sui [a,d,*]

[a] School of Mechanical Engineering Sciences, University of Surrey, Guildford, Surrey GU2 7XH, UK
[b] Science and Technology Facilities Council (STFC), Rutherford Appleton Laboratory, ISIS Facility, Harwell, Oxon OX11 0QX, UK
[c] United Kingdom Atomic Energy Authority, Culham Centre for Fusion Energy, Culham Science Centre, Abingdon, Oxon OX14 3DB, UK
[d] National Physical Laboratory, Hampton Road, Teddington TW11 0LW, UK

ARTICLE INFO

Keywords:
Time of Flight- Neutron Bragg Edge Imaging (TOF-NBEI)
Residual stresses
Characterisation
Neutron analysis
Fusion materials
Texture

ABSTRACT

The European DEMOnstration power plant (EU DEMO) project is currently leading the research endeavours within the fusion field with the goal of developing a next generation fusion reactor. Given the challenging nature of the application, it is essential to establish methodologies that can provide convenient and reliable characterisation of the chosen materials within DEMO. In this paper, the recently developed Time-of-Flight Neutron Bragg Edge Imaging (TOF-NBEI) was used on Tungsten (W)/ Copper (Cu) dissimilar joints sample mock-ups of the cooling system design used in the critical divertor component with the goal of mapping the residual stresses across the sample. Residual strain mapping was performed on the W phase with considerable tensile residual strains identified close to the W-Cu interface. The large-grain microstructure of the Cu phase was analysed using the energy-resolved neutron radiographs. The results will be used as a basis for future TOF-NBEI experiments of tungsten monoblocks related to DEMO.

Introduction

Fusion energy has been a hot topic of discussion in research and science due to its growing potential as an abundant and sustainable energy resource which can benefit humanity in the future [1]. DEMOnstration Power Plant (DEMO) is the next phase in fusion research which will act as a successor to the International Thermonuclear Energy Reactor (ITER) and have a more practical focus on the implementation and applicability of fusion [2,3]. This will also include the assessment of the structural integrity and performance of chosen materials to be used in the reactor which will have to withstand difficult operational conditions such as high heat fluxes (HHF) and plasma bombardments [4,5,6].

One of the essential components of DEMO is the divertor, which is responsible for extracting gas waste and particles, and for protecting the surrounding walls of the reactor from thermal loading. The nature of this application requires strict thermal control, performed by a cooling system of the divertor component with a proposed design of Copper Chromium Zirconium (CuCrZr) cooling pipes and a pure Copper (Cu) interlayer in the middle of a Tungsten (W) block armour to act as a structural heat sink for the divertor. W has shown promise as a plasma facing component (PFC). However, it suffers from a structural point of view due to its brittleness [7]. In addition, the high temperature joining processes currently being considered to create the W/Cu joint will inevitably introduce residual stresses which are further exacerbated by the mismatch in thermal properties between W and Cu [8]. Such residual stresses can influence the mechanical properties, structural integrity, and service life of materials. Hence, being able to accurately determine the impact of these stresses is essential to the structural assessment of the divertor design.

Methodology

The charge neutrality of neutrons and weak interaction with atoms means they can penetrate deep into materials, allowing neutrons to be historically used to probe thick samples [9]. Neutron diffraction has been readily used as an accurate means to obtain residual stress data in a non-destructive manner in a variety of experiments and even as a way of evaluating the reliability of other techniques [10]. More recent

* Corresponding author.
E-mail address: t.sui@surrey.ac.uk (T. Sui).

https://doi.org/10.1016/j.nme.2024.101593
Received 2 October 2023; Received in revised form 15 January 2024; Accepted 18 January 2024
Available online 20 January 2024

advancements in detection technology [11] and the availability of time-of flight (TOF) capabilities at pulsed spallation neutron sources [12] have introduced a new technique known as time-of-flight Neutron Bragg edge imaging (TOF-NBEI) [13], which is based on the same principles as neutron diffraction but with the detection of neutrons in transmission mode instead of diffraction mode. TOF-NBEI has been shown as a viable technique to determine lattice parameters, residual strains [14,15,16], texture [16,17,18] and to evaluate the quality of single-crystals [19,20]. It is also able to map such data across large areas of several square centimeters of a sample with relative ease in comparison to other methods.

Fig. 1 shows a simplified schematic of the imaging experiment and typical data obtained. As for neutron diffraction, Bragg edge imaging makes use of the diffraction phenomenon that occurs when neutrons interact with crystalline materials as described by Bragg's law [21]:

$$\lambda = 2d_{hkl}\sin(\theta) \tag{1}$$

where λ is the neutron wavelength, d_{hkl} is the interplanar spacing for a specific lattice plane (*hkl)* and θ is the Bragg angle. However, in Bragg edge imaging the diffracted neutrons are not measured directly. Instead, the transmission profile for a neutron ray through a sample is analysed as a function of neutron wavelength, providing microstructural information via changes of Bragg edge positions (d_{hkl} values) and changes of relative Bragg edge heights (texture) which can be obtained through fitting an analytical Bragg edge function. A Bragg edge signal for a polycrystalline material is formed through superposition of Bragg dips from individual crystallites. Dips are observed for single crystals or oligo crystals at specific Bragg angles, θ_{dip}, depending on the orientation of the (*hkl*) plane normal to the neutron beam.

As constructive interference and Bragg's diffraction criterion is satisfied for Bragg angles of $\theta = 0°$ to $\theta = 90°$, this is reflected in the transmission profile by a period of steady reduction in the transmission signal as shown in Fig. 1. At Bragg angles $\theta > 90°$, Bragg's law is no longer satisfied which causes a jump in the neutron transmission profile for polycrystalline materials since diffraction no longer occurs for the particular (*hkl*) crystal plane. This sudden spike at a neutron wavelength of $\lambda = 2d_{hkl}$ is what forms the Bragg edge feature in the transmission profile.

One is able to obtain macro-residual strains by assuming elastic distortion of the crystal lattice and considering a stress-free sample using the following equation:

$$\varepsilon = \frac{d_{hkl} - d_{0hkl}}{d_{0hkl}} \tag{2}$$

where ε is the macro-strain and d_{hklo} is the strain free reference lattice spacing. By mapping the Bragg-edge positions across the sample and comparing it with d_{hklo}, the 2D bulk lattice-strain in the direction of the neuron beam through the thickness of the sample can be mapped [22].

In TOF experiments, a wide neutron wavelength range can be considered at once. The neutron wavelength (λ) is calculated using the following equation:

$$\lambda = \frac{hT}{mL} \tag{3}$$

where h is Planck's constant, T is the time of flight of the neutron, m is the mass of the neutron and L is the flight path from neutron source to detector. To measure the wavelength-resolved transmission of the neutrons across the sample, a pixelated neutron detector is used and data are collected once with the sample and another with no sample, also known as 'open beam'. The neutron counts for sample (I) and open beam (I_0) measurements are then used to calculate the thickness-averaged transmission *Tr(λ) (integral through the sample thickness)* using:

$$Tr(\lambda) = \frac{I}{I_o} \tag{4}$$

Pure molten Cu (99.8 % wrt) was cast on a W Monoblock and left to solidify to create the W/Cu sample as seen in the neutron radiograph in

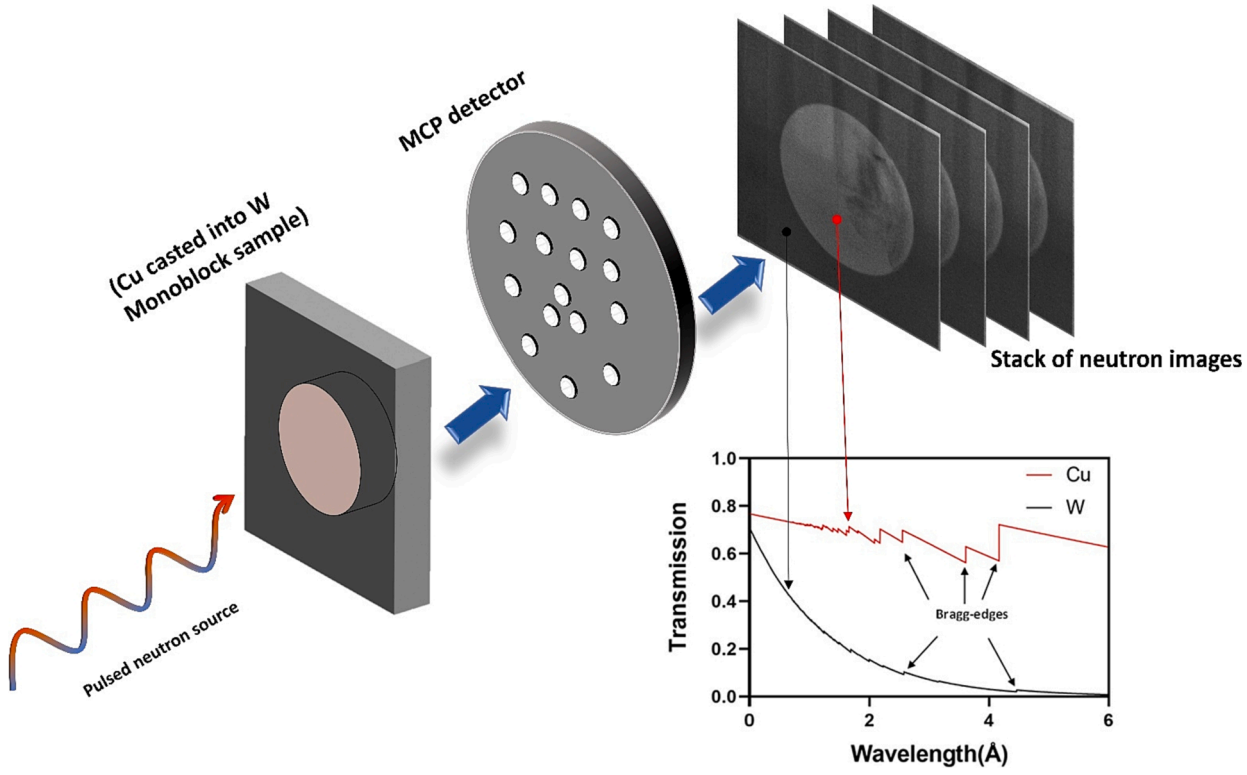

Fig. 1. Schematic of the Neutron Bragg edge experiment and theoretical transmission profiles for non-textured polycrystalline pure Cu and W phases showing the Bragg edge features. Data was obtained using the NXS program [22].

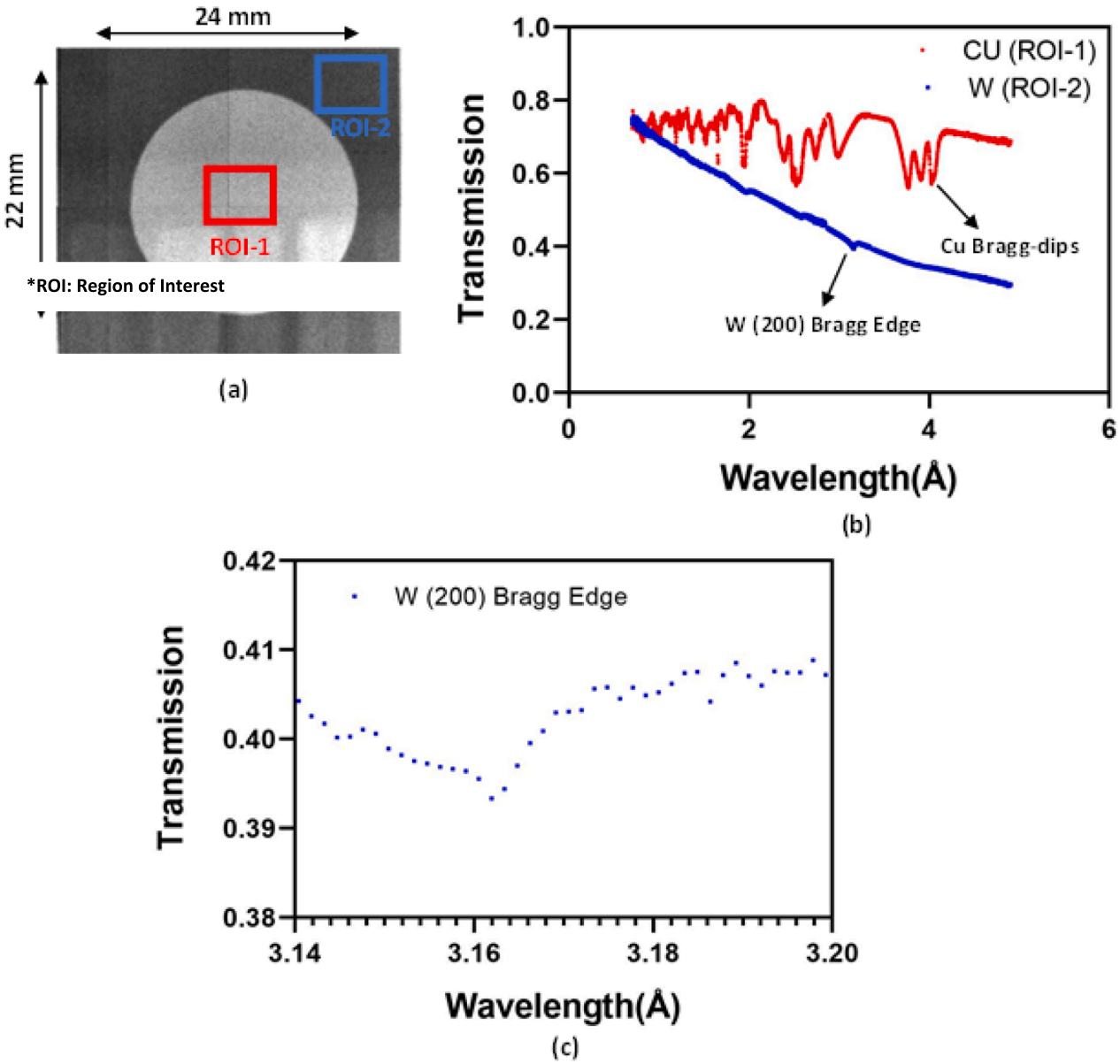

Fig. 2. (a)- Neutron radiograph of the W/Cu sample with the ROIs for the initial transmission analysis. (b) W and Cu transmission profiles showing Cu Bragg dips and W (200) edge. (c)- W (200) edge with greater detail.

Fig. 2(a). More details of the fabrication and preparation of the sample is found elsewhere [23]. The sample dimensions are specified by the manufacturer as 22 × 24 × 4 mm^3 with a Cu radius of 8 mm and thickness of 4 mm. The TOF-NBEI experiment was conducted at the IMAT beamline at ISIS, Rutherford Appleton Laboratory [12,24] with a neutron wavelength range of 0.7–6 Å. The sample was placed 56.5 m from the neutron source (flight path) and a neutron beam collimation ratio L'/D ~ 100 was used with a collimator of diameter (D) of 100 mm at a distance of 10.5 m from the detector. A micro-channel plate (MCP) detector was used to sense the incoming neutrons and subsequently create the neutron radiographic images to be analysed. The detector has a field of view of 28 × 28 mm^2 with a spatial resolution of 55 μm (512 × 512 pixels) [11]; a time binning of 40 μs was used. A total measurement time of 3 h and 1 h was used for sample and open beam measurements, respectively, for an 800 MeV proton beam energy. The TPX_Edge code [25] was used for the data analysis and mapping of the Bragg edges. Firstly, the open beam and sample data were deadtime-corrected, normalised, and cleaned using the ImageJ software [26]. A 5-parameter analytical function was used to perform the Bragg edge curve fitting to determine the position of a single the edge [14]. The strain free reference (d_{hklo}) for W was obtained by determining an average Bragg edge position for regions of interest at the corners of the sample furthest away from the W/Cu interface and assuming that only residual strains due to the thermal mismatch between W and Cu exist in the sample. The mapping of the Bragg edges across the sample was assisted by using a macro-pixel size of 50 × 50 pixels and a running-average with 55 μm step-width. This running average-procedure ensured smoothing of low-transmission, noise-prone data and provided a spatial resolution of about 1.5 mm for the W strain maps.

Further, the bulk texture of the sample was analysed to compliment the obtained Bragg edge imaging results using the GEM diffractometer at the ISIS facility [27].

Results and discussion

The microstructure of the chosen sample presented some challenges for the data analysis. The transmission profiles in Fig. 2 (b) for corresponding W and Cu are shown for ROIs depicted in Fig. 2 (a). Firstly, the

Cu transmission profile exhibits 'Bragg dips' as expected for an oligo/single crystal sample [28]. The principles behind how Bragg dips are formed is similar to that of Bragg edges. However, Bragg dips only occur are specific Bragg angles, θ_{dip}, where the dip position is given by $\lambda = 2d_{hkl}\sin(\theta_{dip})$. This implies large Cu grains in the sample, too few to form the Bragg edge profile seen in polycrystalline materials.

The neutron radiogram stacks were analysed at different TOF as seen in Fig. 3 (a), (b) and (c). The dark regions represent areas of low transmission where Bragg's law is satisfied. Hence, such a dark area indicates the size and shape of a Cu grain in the sample which shows up at a different TOF, i.e. different neutron wavelength, due to a certain grain orientation with respect to the incoming neutron beam and which satisfies the condition for θ_{dip}. Fig. 3 (d) shows transmission profiles taken from regions inside each of the suspected grains considering the (1 1 1) Bragg dip. It is evident that there is a relatively large shift in the dip position between each grain, not caused by macro-strain but by misalignment tilt between the crystals. While the dip position is dependent on both the lattice spacing d_{hkl} and orientation θ_{dip}, it is not possible to analyse the macro-strain. However, it is observed that the dip position does not change within one crystal and the shift in dip position between crystals can be attributed to the change in orientation [28]. In summary, strain mapping cannot be achieved for the Cu region of the sample. Bragg dip Gaussian fitting has been performed in literature [17,18] and is useful for mapping the tilt angles and for testing the quality of single crystals [19].

The W transmission profile in Fig. 2(b) shows few Bragg edges, with the (2 0 0) Bragg edge being the most visible one, while (1 1 0) and (2 1 1) Bragg edges are expected to be stronger for a texture-free, polycrystalline materials (Fig. 1). The (2 0 0) Bragg edge is displayed more clearly in Fig. 2(c). This dominance of the (2 0 0) edge was consistent when surveying regions of interest across the entirety of the W part of the sample indicating a strong alignment of (2 0 0) plane normals along the direction of the neutron beam, since the Bragg edge height is determined by the number of crystallite planes aligned with the normal direction of the sample. Fig. 4 shows the bulk pole figures of the W phase, regenerated from the orientation distribution function measured on the GEM diffractometer. The hot spot with about 6 m.r.d in the middle of the (2 0 0) pole figure confirms the high (2 0 0) texture in agreement with the transmission profile. This data explains the weakness of the (1 1 0) and (2 1 1) Bragg edges in the transmission data.

The (2 0 0) Bragg-edge positions matched well with the theoretical W Bragg-edge position shown in Fig. 1, however with noticeable weak Bragg edges, which is a consequence of the W-neutron interaction, i.e. weak coherent (Bragg) scattering and strong neutron absorption, the latter being responsible for low neutron counts.

Fig. 5 (a) shows (2 0 0) Bragg edge transmission data with corresponding 5 parameter fitting curve and the strain map obtained from the data analysis with an uncertainty error of about 150 με [14]. It is evident that tensile residual strain can be seen in some regions of W close to the interface with Cu. This can be explained when considering the thermal expansion (CTE) of both materials. When the molten Cu is poured onto the W Monoblock, the temperature of the W close to the interface is elevated. Both materials are then left to cool to room temperature. Since Cu has a much higher thermal conductivity, it will exhibit higher cooling rates and tend to contract more than the W. However, the contraction of Cu becomes constrained by the surrounding W causing incompatible strain fields at the interface which are usually accommodated by tensile strains in the lower CTE material (W) and compressive strains in the higher CTE material (Cu). By assuming a biaxial stress state and using Hooke's law, the resultant stresses recorded in the map can reach values exceeding 550 MPa, which is over 40 % of the W yield stress.

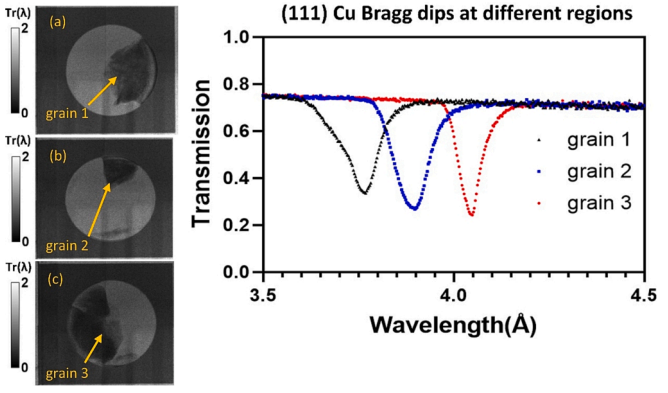

Fig. 3. (a), (b) and (c)- Neutron radiographs at different TOF dark regions representing Cu crystals. (d)- Transmission profiles from regions within each crystal showing Cu (1 1 1) and its shift in position due to the different crystal orientations.

The data obtained does compare well with some other results published in the literature within the scope of the DEMO design material characterisation and testing. Coppola et al conducted neutron diffraction experiments on W diffusion bonded to CuCrZr cooling pipes and found tensile residual stresses in W near the interface in the hoop and axial directions, however at a much lower magnitude below 100 MPa [29] and different lattice planes were considered for measurements. Moreover, tensile residual stresses are also known to be contributors to stress corrosion cracking and reduce the fatigue life of components. This further emphasises the importance of obtained results within the scope of the divertor structural assessment and joining procedures of dissimilar materials, which will be used as the basis and guidelines for future TOF-NBEI experiments on samples that consider the working conditions such as HHF and plasma bombardments. Furthermore, such samples have been known to undergo significant microstructural changes such as recrystallisation [6]. This can also be evaluated comprehensively across the entirety of samples using Bragg edge height fitting and mapping, emphasising the potential of TOF-NBEI in the context fusion materials research.

Conclusion

The following experimental conclusions can be made based on the presented data:

- TOF-NBEI was successfully used to map the 2D macrostrain for the W region in the W/Cu sample. Considerable tensile residual strains are observed near the interface in the direction of the neutron beam through the sample.
- The Cu region consists of a few grains, insufficient to produce the Bragg edge profiles necessary for the strain analysis. Bragg- dips were observed instead which help characterise crystallite shapes and orientations.
- Pole figures from neutron diffraction support the TOF-NBEI W transmission results, showing a strong preferential alignment of (2 0 0) planes along the normal direction of the sample.
- Data obtained will contribute to the residual stress characterisation methodologies within the scope of DEMO.

To the best of the authors' knowledge, Bragg edge fitting of W Bragg edges is reported here for the first time, even though the analysis was bedevilled by low counting statistics.

CRediT authorship contribution statement

Omar Mohamed: Conceptualization, Visualization, Writing – original draft. **Bin Zhu:** Investigation, Writing – review & editing. **Nathanael Leung:** Investigation. **Winfried Kockelmann:** Investigation, Methodology, Writing – review & editing. **Thomas R. Barrett:** Sample fabrication, Resources. **Mark J. Whiting:** Supervision. **Yiqiang Wang:**

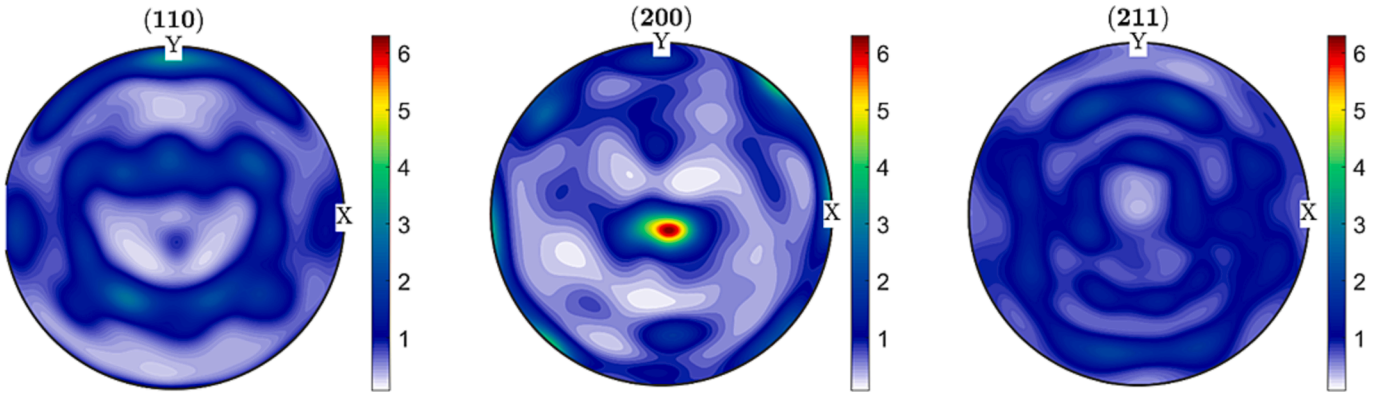

Fig. 4. Pole figures generated from the GEM diffraction data showing strong (200) pole densities.

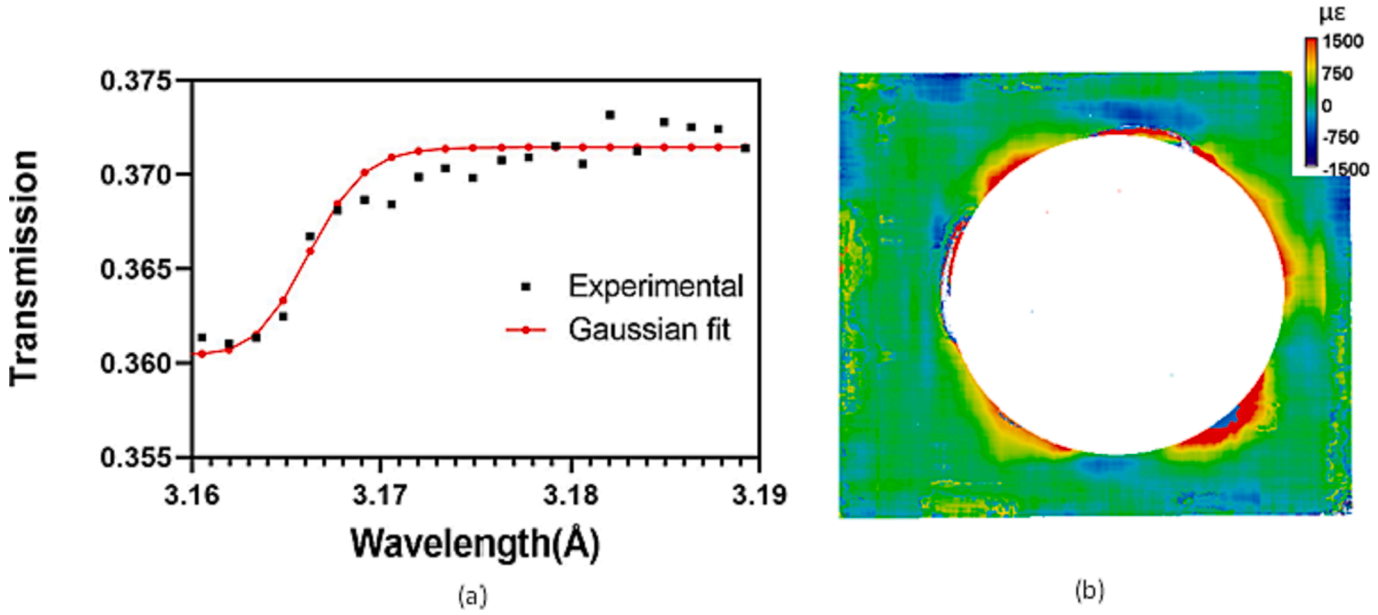

Fig. 5. (a)- Analytical fitting curve of the (200) W Bragg edge. (b)- Strain map obtained for the W part of the sample.

Conceptualization, Funding acquisition, Supervision, Writing – review & editing. **Tan Sui:** Conceptualization, Funding acquisition, Supervision, Writing – review & editing.

Declaration of competing interest

The authors declare that they have no known competing financial interests or personal relationships that could have appeared to influence the work reported in this paper.

Data availability

Data will be made available on request.

Acknowledgement

Dr Yiqiang Wang and Dr Thomas R. Barrett would like to acknowledge the EPSRC Fusion Grant [grant number EP/W006839/1]. The authors thank the ISIS neutron and muon source for providing the beamtime at IMAT (DOI:10.5286/ISIS.E.RB1920513) facilities. The Doctoral College Studentship Award 4 (DCSA4) of the University of Surrey is acknowledged for the funding support. Dr Sui would like to acknowledge funding from the Royal Academy of Engineering under the Industrial Fellowships programme.

References

[1] F. Romanelli, L.H. Federici, R. Neu, D. Stork, H. Zohm, A roadmap to the realization of fusion energy, in: Proc. IEEE 25th Symp. Fusion Eng., Jan. 2013, pp. 1–4.
[2] H. Yamada, et al., Japanese endeavors to establish technological bases for DEMO, Fusion Eng. Des. 109–111 (Nov. 2016) 1318–1325, https://doi.org/10.1016/J.FUSENGDES.2015.12.035.
[3] S. Matsuda, K. Tobita, Evolution of the ITER program and prospect for the next-step fusion DEMO reactors: status of the fusion energy R&D as ultimate source of energy, J. Nucl. Sci. Technol. 50 (4) (Apr. 2013) 321–345, https://doi.org/10.1080/00223131.2013.773166.
[4] J.H. You et al., Conceptual design studies for the European DEMO divertor: Rationale and first results, Fusion Eng. Des., 109–111(PartB) (Nov. 2016) 1598–1603, doi: 10.1016/J.FUSENGDES.2015.11.012.
[5] L. Commin et al., Assessment of Copper based Materials for the Water-Cooled Divertor Concept of the DEMO European Fusion Reactor, 2013. doi: 10.1109/SOFE.2013.6635275.un.
[6] J.H. You, et al., High-heat-flux technologies for the European demo divertor targets: State-of-the-art and a review of the latest testing campaign, J. Nucl. Mater. 544 (Feb. 2021) 152670, https://doi.org/10.1016/J.JNUCMAT.2020.152670.
[7] T. Zhang, Z. Xie, C. Liu, Y. Xiong, "The Tungsten-Based Plasma-Facing Materials", in Fusion Energy, IntechOpen (2020), https://doi.org/10.5772/intechopen.88029.
[8] D. Easton, J. Wood, S. Rahimi, A. Galloway, Y. Zhang, C. Hardie, Residual Stress Generation in Brazed Tungsten Dissimilar Joints; Residual Stress Generation in Brazed Tungsten Dissimilar Joints, IEEE Trans. Plasma Sci. 44 (9) (2016) 1625, https://doi.org/10.1109/TPS.2016.2565205.

[9] G. S. Schajer, Ed., Practical Residual Stress Measurement Methods, Wiley, 2013, doi: 10.1002/9781118402832.
[10] M. Haghshenas, Assessing residual stresses in friction stir welding: neutron diffraction and nanoindentation methods, Int. J. Adv. Manuf. Technol. 93 (Dec. 2017), https://doi.org/10.1007/s00170-017-0759-2.
[11] A.S. Tremsin, et al., High-resolution strain mapping through time-of-flight neutron transmission diffraction with a microchannel plate neutron counting detector, Strain 48 (4) (Aug. 2012) 296–305, https://doi.org/10.1111/j.1475-1305.2011.00823.x.
[12] W. Kockelmann, S.Y. Zhang, J.F. Kelleher, J.B. Nightingale, G. Burca, J.A. James, IMAT – a new imaging and diffraction instrument at ISIS, Phys Procedia 43 (Jan. 2013) 100–110, https://doi.org/10.1016/J.PHPRO.2013.03.013.
[13] J.R. Santisteban, L. Edwards, M.E. Fizpatrick, A. Steuwer, P.J. Withers, Engineering applications of Bragg-edge neutron transmission, Appl. Phys. A Mater. Sci. Process, 74(SUPPL.II) (Dec. 2002), doi: 10.1007/s003390101241.
[14] R.S. Ramadhan, et al., Characterization and application of Bragg-edge transmission imaging for strain measurement and crystallographic analysis on the IMAT beamline, J Appl. Crystallogr. 52 (2) (Apr. 2019) 351–368, https://doi.org/10.1107/S1600576719001730.
[15] R. Woracek et al., Neutron Bragg-edge-imaging for strain mapping under in situ tensile loading, J. Appl. Phys, 109(9) (May 2011), doi: 10.1063/1.3582138.
[16] Y. Su, et al., Neutron Bragg-edge transmission imaging for microstructure and residual strain in induction hardened gears, Sci. Rep. 11 (1) (2021) Dec, https://doi.org/10.1038/s41598-021-83555-9.
[17] Y. Sakurai, H. Sato, N. Adachi, S. Morooka, Y. Todaka, and T. Kamiyama, "Analysis and mapping of detailed inner information of crystalline grain by wavelength-resolved neutron transmission imaging with individual bragg-dip profile-fitting analysis," Applied Sciences (Switzerland), vol. 11, no. 11, Jun. 2021, doi: 10.3390/app11115219.
[18] H. Sato, et al., Inverse pole figure mapping of bulk crystalline grains in a polycrystalline steel plate by pulsed neutron Bragg-dip transmission imaging, J. Appl. Crystallogr. 50 (6) (Dec. 2017) 1601–1610, https://doi.org/10.1107/S1600576717012900.
[19] K. Watanabe, K. Matsumoto, A. Unitani, K. Hitomi, M. Nogami, W. Kockelmann, Crystalline characterization of TlBr semiconductor detectors using wavelength-resolved neutron imaging, Sensors and Materials 32 (4) (Apr. 2020) 1435–1443, https://doi.org/10.18494/SAM.2020.2744.
[20] J. Strickland, et al., 2D single crystal Bragg-dip mapping by time-of-flight energy-resolved neutron imaging on IMAT@ISIS, Sci. Rep. 10 (1) (2020) Dec, https://doi.org/10.1038/s41598-020-77572-3.
[21] C. Elliott and F. W. Poos, Crystal Structure: The Crystalline State, Edited by Sir W. H. Bragg and W. L. Bragg. Vol. I. A General Survey, by W. L. Bragg, xiv + 352 pages, 23 × 14.5 cm, with 186 figures and 6 appendices. Published by Macmillan and Company, 60 Fifth Ave., New York City, 1934, $5.50.," Science (1979), vol. 80, no. 2074, pp. 290–291, Sep. 1934, doi: 10.1126/SCIENCE.80.2074.290.B.
[22] M. Boin, Nxs: A program library for neutron cross section calculations, J. Appl. Crystallogr. 45 (3) (Jun. 2012) 603–607, https://doi.org/10.1107/S0021889812016056.
[23] E. Bang, H.C. Kim, K. Kim, J. Choi, S.H. Hong, Gas pressure casting technique for manufacturing of W/OFHC-Cu monoblock, Fusion Eng. Des. 176 (Mar. 2022), https://doi.org/10.1016/J.FUSENGDES.2022.113021.
[24] T. Minniti, K. Watanabe, G. Burca, D.E. Pooley, W. Kockelmann, Characterization of the new neutron imaging and materials science facility IMAT, Nucl. Instrum. Methods Phys. Res A 888 (Apr. 2018) 184–195, https://doi.org/10.1016/J.NIMA.2018.01.037.
[25] A.S. 'Tremsin, TOF Analysis code, Private Communications, 2023.
[26] J. Schindelin, et al., Fiji: an open-source platform for biological-image analysis, Nat. Methods 9 (7) (Jul. 2012) 676–682, https://doi.org/10.1038/nmeth.2019.
[27] W. Kockelmann, L. C. Chapon, and P. G. Radaelli, "Neutron texture analysis on GEM at ISIS," Physica B Condens Matter, vol. 385-386 I, pp. 639–643, Nov. 2006, doi: 10.1016/j.physb.2006.06.091.
[28] H. Sato, Deriving quantitative crystallographic information from the wavelength-resolved neutron transmission analysis performed in imaging mode, J. Imaging, 4 (1) (2018). MDPI Multidisciplinary Digital Publishing Institute, doi: 10.3390/jimaging4010007.
[29] R. Coppola, et al., Neutron diffraction measurement of residual stresses in an ITER-like tungsten-monoblock type plasma-facing component, Fusion Eng. Des. 146 (Sep. 2019) 701–704, https://doi.org/10.1016/J.FUSENGDES.2019.01.059.